



Full Length Article



Investigating the oxidative reactivity and nanostructural characteristics of diffusion flame generated soot using methyl crotonate and methyl butyrate blended diesel fuels

Samantha Da Costa^a, Akshay Salkar^a, Anand Krishnasamy^b, Ravi Fernandes^c,
Pranay Morajkar^{a,*}

^a School of Chemical Sciences, Goa University, Taleigao Plateau, 403206 Goa, India

^b Internal Combustion Engines Laboratory, Indian Institute of Technology Madras, India

^c Thermophysical Quantities, Physikalisch-Technische Bundesanstalt 38116 Braunschweig, Germany

ARTICLE INFO

Keywords:

Soot
Nanostructure
Biofuel surrogates
Combustion
Oxidative reactivity

ABSTRACT

Combustion-generated particulate matter has a consequential fallout on climate, environment, and human health. Thus, comprehension of soot formation and mitigation processes using biodiesel additives is a focal point of modern combustion research. This study presents an intricate investigation of enhanced oxidative reactivity and its dependence on the soot nanostructural properties induced by distinctive blending of a saturated and an unsaturated biodiesel surrogates namely, methyl butyrate (MB) and methyl crotonate (MC) respectively with pure diesel. 25% MB-75% diesel fuel resulted in the lowest sooting propensity and lowest activation energy (155.4 ± 2 kJ/mol) for soot oxidation in comparison to pure diesel fuel and diesel soot (175.1 ± 2 kJ/mol). The soot was collected using a smoke point apparatus involving a wick-fed laminar diffusion flame at atmospheric pressure after meticulous observation of the smoke points. The detailed nanostructural characterization of the flame generated soots were performed using high-resolution transmission electron microscopy, X-ray diffraction, elemental analysis and Raman spectroscopy. BET surface area analysis, and thermogravimetric analysis were carried out for surface area distinction and activation energy calculations respectively. It revealed that, addition of MB to diesel resulted in improved fuel combustion with reduction in primary soot particle diameter, greater inter-planar separation, increased fringe tortuosity and greater crystal structure disorder resulting in its enhanced reactivity with O₂. The 25% MC-75% diesel blend resulted in relatively greater sooting propensity while its soot exhibited lower crystal structure disorder and greater activation energy (165.0 ± 2 kJ/mol) for O₂ induced oxidation compared to 25% MB-75% diesel, possibly due to the resonance stabilized radical (RSRs) formation that altered the fuel combustion chemistry. Therefore, this study successfully depicts that the structural differences in the surrogate fuels do influence the soot formation and oxidation kinetics. These structural effects therefore need to be considered when formulating the global multiphase kinetic models for biodiesel-diesel fuel combustion.¹

1. Introduction

Over the years, increased use of fossil fuels has resulted in reduced air quality, global warming and climate change which now threatens the very existence of life on earth. A huge research contribution has been made towards the study of air pollutants especially those in the gas phase. Particulate matter (PM), although insignificant in comparison to the volume of the gaseous pollutants, is also an airborne ecology

wrecker. In a recent study by Islam et al. [1] reported that the PM at an urban traffic hub in India is about $126.76 \mu\text{g}/\text{m}^3$ [3]. The presence of such PM in the atmosphere leads to cytotoxicity and consequently stimulates genotoxicity to human health [1]. These PMs are formed out of PAH's (Polycyclic aromatic hydrocarbons), which are potent mutagens and carcinogens. These not only affect the living organisms but also cause deleterious environmental complications such as regional global warming, leading to the melting of polar ice caps and a subsequent rise

* Corresponding author.

E-mail address: pranay@unigoa.ac.in (P. Morajkar).

¹ Dedicated to Prof. Purnakala Samant on the occasion of her 50th birthday celebration.

in sea levels, making it a vicious circle of ecological damage [2–4].

Several engine design modifications have been implemented so far to reduce the pollutant emissions without compromising on combustion efficiency. However, there has been a classic trade-off either to reduce nitrogen oxides (NO_x) and increase PM or vice versa [5–7]. Mitigation of soot in particular has seen a limited success rate so far. One of the recently adopted effective strategy includes the use of suitable fuel additives to decrease soot production and improve soot oxidation rate within the combustion engines. Subsequently, the use of diesel particulate filters (DPF's) and its effective regeneration strategy for post combustion treatment is also desired. The finest and most accepted way to achieve this is to modify the fuel with easily available renewable additives such as biofuels. Morajkar et al. [3,8–10] and Abdrabou et al. [3,8,10], among others, have explored the effect of adding biofuels such as Karanja, Jatropha, Camphor oil, etc., to diesel and their impact on soot nanostructure and its oxidative reactivity for improved regeneration of DPFs. The addition of these biodiesel additives resulted in several favourable properties in soot particles, such as increased structural disorder, decreased primary particle size, and higher percentages of oxygen functionalities in the soot structure. A notable degree of disorder in the soot nanostructure leads to greater susceptibility towards an attack by O_2 and various other radicals during the combustion process [3,8–10].

Biodiesels are a complex mixture of fatty acid methyl esters (FAME), which are most often obtained from vegetable and seed oils, used cooking vegetable and animal fats. It is produced by employing a transesterification reaction and further refining it to remove any unwanted particulates [11]. A study by Jiang et al. [12] suggested that the oxygenated biofuels facilitate efficient combustion and also help in reducing pollution by altering the physical and chemical characteristics of soot particles. Also, the change in density and kinematic viscosity play a fundamental role in stimulating the oxidation of the fuel, thus lowering the soot production rate. Schönborn et al. [13] recommended three discrete features of the biodiesel molecular structure, given as, the fatty acid chain length, extent of unsaturation and alcohol chain length [13,14]. A number of studies have highlighted that a decreased exhaust soot production rate corresponds to the oxygen content in the fuel. The simultaneous use of oxygenated additives not only decreases the soot emissions but also results in a decrease in CO and HC emissions due to improvement in combustion efficiency [15]. The presence of internal fuel bound oxygen leads to faster fuel oxidation rates and the possibility to burn more fuel at the same stoichiometry [16,17]. Oxygenated fuels eliminates the inhomogeneity in fuel/oxidant ratio thus enhancing internal combustion of the fuel. This not only reduces the soot formation kinetics but also enhances the internal soot oxidation reactions, which leads to greater disordered soot with a reduction in primary particle size. Such smaller soot particles have higher number of exposed carbon atoms on their surfaces allowing easy oxidation by O_2 /radicals, further increasing their reactivity and oxidation rates. Such effects on fuel bound oxygen on soot particle diameter has been well presented in the works of Abdrabou et al. [3], Morajkar et al. [9] etc. and an elaborated discussion can be found in the literature for further reading [18–20].

For instance, Verma et al. [21] observed that blending of oxygenated additives decreased the soot primary particle size, promoted oxidation of soot particles, resulted in fringes with more curvature which greatly contributed to faster soot oxidation [21]. Kholghy et al. [22] carried out an experimental study to evaluate the structural effects of unsaturation in biodiesels. The study marked that the existence of an ester group quenches soot formation; however, unsaturation remarkably stimulates soot inception and development, promoting larger primary soot particles. All these factors influence the efficacy of soot mitigation, and hence the chemical and structural properties of the biodiesel must be evaluated before blending them with fossil fuels for engine applications.

Furthermore, addition of biodiesels to diesel fuel results in a highly complex combustion chemistry. This makes understanding their reaction rates and construction of kinetic models a very challenging task

with high degrees of uncertainties especially with respect to the multi-phase chemistry in engines and flames. To improve the engine efficiency using biodiesel fuels, it is of utmost importance to construct predictive gas phase combustion kinetic model, which is currently being achieved using biodiesel surrogate fuels. The ester group COOR, is an oxygen functional group and an unsaturated ester such as methyl crotonate (MC) and a saturated ester such as methyl butyrate (MB) act as suitable surrogate fuel additives to investigate biodiesel -diesel fuel combustion chemistry. The chemical structures of MB and MC differ by the presence of an unsaturated C=C double bond in MC molecules, and both contain two oxygen atoms and can have differing effects on combustion properties of the blends [12]. Lele et al. [23] have developed a compact kinetic model for MB oxidation in shock tubes, laminar and counter-flow diffusion flames etc. The study also pointed out the propriety of MB as a suitable biodiesel surrogate fuel. An experimental and kinetic modelling study by Vallabhuni et al. [24] highlights the influence of these surrogates on auto-ignition characteristic of the fuel in gas phase. However, these models lack any information on their effects on PM i.e. soot and affects the construction of multiphase kinetic models.

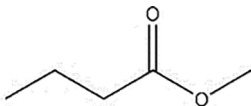
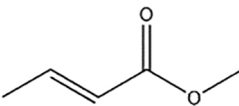
Although the physical and chemical properties of these surrogates are well described in the literature, their impact on diesel soot formation chemistry and subsequent oxidative reactivity of the generated soot is barely understood. Till date, there is only one study highlighting the impact on sooting propensity due to the MB and MC addition to an ethylene inverse diffusion flame available in the literature [12]. However, the impact of MB and MC on diesel fuel, its sooting tendency, diesel soot nanostructural disorder and the subsequent oxidative reactivity of the combustion generated soot is not reported till date to the best of our knowledge. In our earlier study, it has been demonstrated that the bio-fuel/diesel blend generated soot nanostructure and its oxidative reactivity studies of flame regenerated soot (using smoke point apparatus) is comparable to that of a CI engine generated soot and hence can be used as a validated method to other such biofuels and their blends with diesel [10]. Therefore, in this study, sooting propensity measurements with pure diesel, MB-diesel and MC-diesel blends have been performed in a smoke point apparatus. The impact of MB and MC addition to diesel on soot nanostructure and its oxidative reactivity in air with reference to applications in diesel particulate filter regeneration has been investigated using several material characterization techniques. All these results are discussed in detail in the subsequent sections.

2. Experimental particulars

2.1. Fuel characteristics

The analysis was carried out using commercial diesel fuel procured from a local commercial fuel station from Panaji, Goa, India, and the surrogate chemicals methyl butyrate (MB) (98%) and methyl crotonate (MC) (98%) were purchased from Alfa Aesar and Sigma Aldrich respectively. The surrogates were effortlessly miscible with the diesel fuel without phase separation. The fuel characteristics of biodiesel surrogates blended with diesel were determined incisively, as presented in Table 1. The kinematic viscosity of the diesel fuel and the blends were systematically determined using a digital rotating viscometer (Anton Par) observing the procedure consistent with the ASTM D445 standard and the density was measured using a digital oscillating U-tube (Anton Par) [10]. As these surrogate fuels of lower viscosity are blended with diesel having a higher viscosity, consequently, the viscosity of the blends dropped below that of pure diesel fuel. The interdependence of density and viscosity is inversely proportional, and the values are evident from Table 1 [25,26]. The calorific values were measured using a digital bomb calorimeter (IKA C2000) and lower calorific value was observed for the blends compared to pure diesel fuel [10]. A detailed description of these measurement techniques is available in the supplementary section. The fuel blends MBD, MCD, and D were prepared by volume basis and correspond to methyl butyrate - diesel blend, methyl crotonate

Table 1
Physicochemical properties and fuel characteristics.

Physical properties	25% Methyl Butyrate- 75% Diesel blend (MBD-25)	25% Methyl Crotonate-75% Diesel blend (MCD-25)	Diesel (D)
	 Methyl butyrate	 Methyl crotonate	
Density (g/cc) @20 °C	0.840	0.850	0.726
Kinematic viscosity (cSt) @ 20 °C	2.160	2.137	4.239
Calorific value (kJ/kg)	39,590	36,763	44,898
Soot production rate (mg/h)	0.85	1.20	5.40
#Fuel flow rate (g/s)	0.001620	0.001664	0.001274

#Obtained from the calibration plot shown in [supplementary fig. S2](#).

- diesel blend, and pure diesel, respectively. The 25% methyl butyrate and 75% diesel blend and the 25% methyl crotonate and 75% diesel blend was coded as MBD-25 and MCD-25. Henceforth these notations will be used to refer to the particular blend being discussed. As observed from the values specified in [Table 1](#), the soot production rate of the blends is fairly lowered in comparison to the pure diesel fuel [27]. The soot production rate of saturated MBD-25 is lower than that of MCD-25 by 0.35 mg/h and lower than D by 4.55 mg/h. The fuel properties will be further discussed in subsequent sections. All tests were run using the same batch of fuels to ensure consistency in the results.

2.2. Smoke point apparatus and soot collection

Smoke point apparatus has widely been used to test the soot-producing characteristics or sooting propensity of the fuel before they can be tested in engines. This approach is free from other interfering components such as lubricating oil, specs of rust, trace metals and other particles that end up in the combustion system of engines [10]. The smoke point apparatus can be adequately used to mimic a diesel engine concerning to a specified set of combustion conditions and can be finetuned to study sooting properties of the fuel blends under investigation. An image of the diffusion flame setup/smoke point apparatus has been added in the supplementary section, [fig. S1](#). The apparatus used in this study, was purchased from Petro-Diesel Instruments Company, West Bengal, India, bearing the product code PDIC-SP021 as per ASTM D-1322. It consists of a cylindrical fuel reservoir into which the measured amount of fuel is filled (10 ml), and a cotton wick is soaked in the required fuel blend and inserted into the wick tube. Flame adjustment knob allows controlled variation in wick exposure and flame height. The tip of this wick is then flared up to ignite the flame. The flame is concealed in a metallic chamber, with a scale in mm placed at the rear of the flame such that it can easily be read through the transparent glass window. A chimney at the upper end of the smoke point apparatus consists of a perpendicular microfiber inline filter assembly (PEIF06GA, Presshot Engineers, Maharashtra, India) of 70 mm diameter, enclosed in a high temperature silicon gasket encased in a stainless steel (SS316) filter casing. The soot was deposited on a glass microfiber filter (Whatman). The vacuum suction pump connected at the exit end aids in the soot collection. The smoke points were determined by observing the wings of the flame precisely with a magnifying glass and was noted once the flame was stabilised at a given flame height within a few minutes [28–31]. To produce enough soot for characterization, the flame height was regulated at 2 mm above the smoke point value. The microfiber soot collection filters were changed at regular intervals to avoid soot agglomeration and particle growth by coagulation. The soot collection process was repeated thrice for each fuel sample, the filters were dried and the soot was scrapped out carefully. An analytically acceptable sample of soot was prepared using coning and quartering method (elaborated in section 3 of [supplementary file](#)) for further

characterization [32].

For pure diesel, soot was collected at 21 mm, and for MBD-25 and MCD-25, it was collected at 28 and 27 mm, respectively with an error bar of ± 1 . The collected soot was dried at a constant temperature of 250 °C in a tubular furnace with continuous nitrogen flow for 1 h, to clear away any adsorbed volatiles and was further subjected to material characterization. This soot was stored in an inert atmosphere for further analysis.

2.3. Material characterization

The soot samples collected from pure diesel, MBD-25, and MCD-25 were subjected to morphological and chemical characterization. The crystallographic structure at the nanoscale was analysed using FEI Tecnai G20 scanning HRTEM operated at 300 kV. The soot samples were dispersed in acetone and sonicated for 10 min. The sample was then coated on a Lacey carbon-coated, 400 mesh copper grid and air-dried under an infrared lamp. The oxidation properties of soot samples were studied with the aid of a thermogravimetric analyser (TGA, NETZSCH STA 409PC-LUXX). The dried soot samples were heated in air from 300 to 800 °C at distinct temperature-programmed heating rates of 3, 5, 7, and 9 °C. The quantitative particulars such as length of the PAH, thickness or height of the PAH stack, and spacing between layers were calculated using powder X-ray diffraction (XRD) (Philips PW-1840, Cu K α , $k = 0.154$ nm). The structural disorder in the soot samples was further analysed using a Raman spectrometer (LAB RAM HR Horiba, France) equipped with a 532 nm Nd-YAG laser 100 mW and lateral resolution of ~ 5 μ m. Elemental analysis (C, H, N, S) were performed on a calibrated Elemental Vario Micro Cube CHNS analyser and SEM-Carl Zeiss (JSM-5800LV) coupled with Ametex EDX PV6500 system elemental analyser. The Brunauer-Emmett-Teller (BET) N₂ adsorption-desorption isotherms were recorded using Autosorb IQ QUA 211011. The dried soot samples were weighed (100 mg each) in a quartz sample tube. Prior to isothermal analysis the already dried soot samples were degassed under vacuum (0.01 mbar) at 120 °C for 2 h to remove even the atmospherically adsorbed gases. The degassed samples were then subjected to a 20 point BET isotherm measurements at a temperature of -196 °C using a liquid nitrogen bath and the surface area was calculate by the program based on the BET equation.

3. Results and discussion

3.1. Fuel properties and sooting propensity of fuels

Fuel properties discussed in [Table 1](#) have significant effects on the start of combustion and fuel consumption, influencing the emissions and other efficiency-related characteristics. The lower viscosity of the blends in comparison to diesel stimulates efficient atomization of the fuel blend, and the surrogate fuels being conveniently miscible in diesel

develop into a favourable homogeneously combusting flame [33]. Atabani et al. [34] indicated that the calorific values of biodiesels are lower than diesel due to their higher oxygen content. As the surrogate fuels have a higher percentage of oxygen in comparison to pure diesel, where C and H are dominant species, the blends exhibit lower calorific values in comparison to diesel fuel [35,36]. Also, the blending of oxygenated fuels such as palm oil [37], camphor oil [9], Jatropha [10,38], Karanja [8,39], castor oil [40] etc. in similar flame studies have been found to reduce the soot production rate, which is similar to the trends observed on addition of surrogate fuels to diesel. Adding oxygenated additives into pure diesel conceivably enhances fuel oxidation due to the effective combustion of fuel and further restrict soot generation [9,41]. The lowering of soot production rate in MBD-25 in contrast to MCD-25 could be due to the greater stability of the resonance stabilised radicals (RSR's) formed in the MCD-25 flame. These RSR's have been detected and their stabilization effect has studied by Gaïl et al. [42], Teruel et al. [43] and several others for gas phase reaction kinetics.

Encapsulating the fuel properties when surrogate fuels are blended with diesel, they decrease viscosity, allow homogeneous mixing and induces internal fuel oxidation, thus improving the combustion efficiency. Furthermore, among the surrogate fuels, the soot production rate is noticeably higher in MCD-25 in comparison to MBD-25. The presence of fuel-bound oxygen and other favourable physicochemical properties of the blended fuels favour effective oxidation of the fuel which is attributed to the decrease of the sooting propensity of the flame [44,45]. In order to further analyse the physical and nanostructural features of the soot produced by these blends, flame studies were carried out to find an ideal smoke point at which soot collection could be carried out (Fig. 1).

Measurement of the smoke point of the fuel gives a direct measure of the sooting propensity of the fuels. The smoke point of pure diesel was determined to be 19 mm, while MBD-25 and MCD-25 show optimum mean smoke point values of 26.3 and 25.2 mm respectively with an error bar of (± 0.5 mm). The inference from the smoke point values suggests that the flame height initially is found to increase with the addition of the surrogate fuels to diesel, it reaches a maximum value at 25% blending of surrogate fuels with diesel. Further addition of surrogate fuels results in a decrease in flame height. An increment in the smoke point signifies that a higher flame height or greater fuel flow rate is required to generate soot particles. Thus the sooting propensity of diesel is lowered in the following order Diesel > MCD-25 > MBD-25 [3].

The production and physicochemical properties of soot reasonably rely on the fuel mass flow rate. In this study, the fuel mass flow rate of

MBD-25, MCD-25, and D was determined by monitoring the weight loss of the fuel contained in the reservoir as a function of time for flame heights fixed at 10, 20, and 30 mm using an analytical balance. The values obtained for each fuel were plotted against time to obtain distinguished linearity, and the slope of these plots corresponded to the fuel mass flow rate. The actual fuel flow rates at the experimental conditions of soot collection, for each fuel was then obtained from the linear regression fit of the calibration plot at the respective flame heights. The plot is presented in the supplementary fig. S2. The values were found to be fairly constant within the error limits $\pm 0.1 \times 10^{-3}$ g/s for all three fuels at a given flame height [46]. The collected soot samples were subjected to oxidative reactivity studies with O_2 to get an insight into the surrogate fuel induced differential chemical reactivity of soot samples. Furthermore, these studies are desired for understanding the soot mitigation efficiencies in DPF technologies.

3.2. Oxidative reactivity studies of soots

Thermogravimetric analysis (TGA) serves as an essential technique for the analysis of soot oxidation kinetics, as the oxidative response is directly related to its reactivity with O_2 . Thermogravimetric analysis is carried out in zero air to inspect the oxygen-stimulated soot oxidation. Such analysis provides an insight into the oxidation of soot which is essential to boost the regeneration of DPF's [10]. The soot conversion (α) is given in eq. 1 and is measured as a function of temperature at varied heating rates of 3, 5, 7, and 9 $^\circ\text{C}/\text{min}$.

$$\alpha = \frac{(M_o - M_T)}{(M_o - M_L)} \quad (2)$$

where M_o , M_T , and M_L correspond to initial soot mass, partially oxidized soot mass, and leftover soot mass consisting mainly of ash. A comparative analysis of the soot conversion, α measured at a fixed heating rate of 7 $^\circ\text{C min}^{-1}$ has been included for enhanced clarity as fig. S3 in the supplementary section. The activation energy, E_a , of this oxidation process is computed using the Friedman method [47–48]. The rate of soot conversion $\left(\frac{d\alpha}{dt}\right)$ and soot conversion (α) can be correlated using the following equation.

$$\left(\frac{d\alpha}{dt}\right) = k(T)f(\alpha) \quad (3)$$

where $k(T)$ is the rate constant indicated by the Arrhenius equation, $k = Ae^{-\left(\frac{E_a}{RT}\right)}$. E_a is the activation energy, A and T are the pre-exponential factor and temperature of soot oxidation, respectively. The reaction model or conversion function is given by $f(\alpha)$, this term rules out the requirement for detailed individual oxidation reactions as the concentration of O_2 is kept steady through the TGA experiments.

The soot conversion rate quantified in air at different heating rates is given in Fig. 2 while the activation energies at several conversion levels and temperatures are calculated and expressed in Fig. 2G. It is observed that as the heating rate increases, the soot conversion curve shifts towards higher temperatures. This could well be a consequence of the presence of a temperature gradient between the carbon sample and the air resulting from a heat transfer delay. Also, during the heating process, the time available for the sample to reach a given temperature and interact with O_2 at that particular temperature is shortened gradually as the heating rate increases [49]. Therefore, a combination of different heating rates and collective analysis of the effects are adequately accounted for, thereby proving higher accuracy in activation energy calculations.

From the plot of activation energy at different conversion levels as a function of temperature, it can be perceived that at low conversion levels, i.e., up to 0.15, the activation energies of the three soot samples

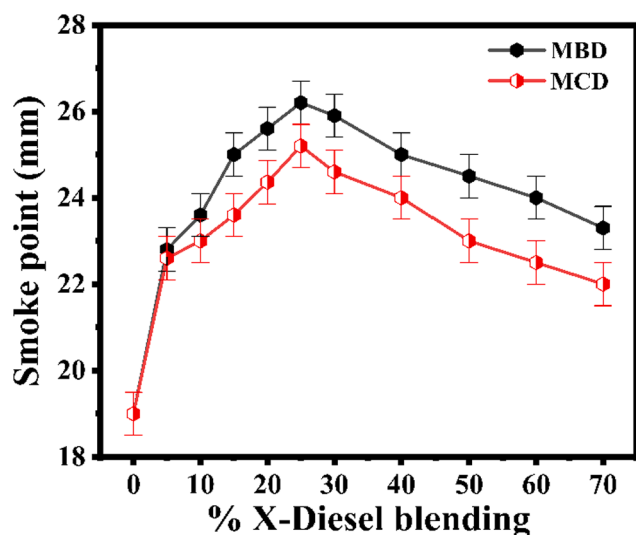


Fig. 1. Variation in smoke point with various blending percentages (% X) of Methyl Butyrate (MBD) and Methyl Crotonate (MCD) with diesel.

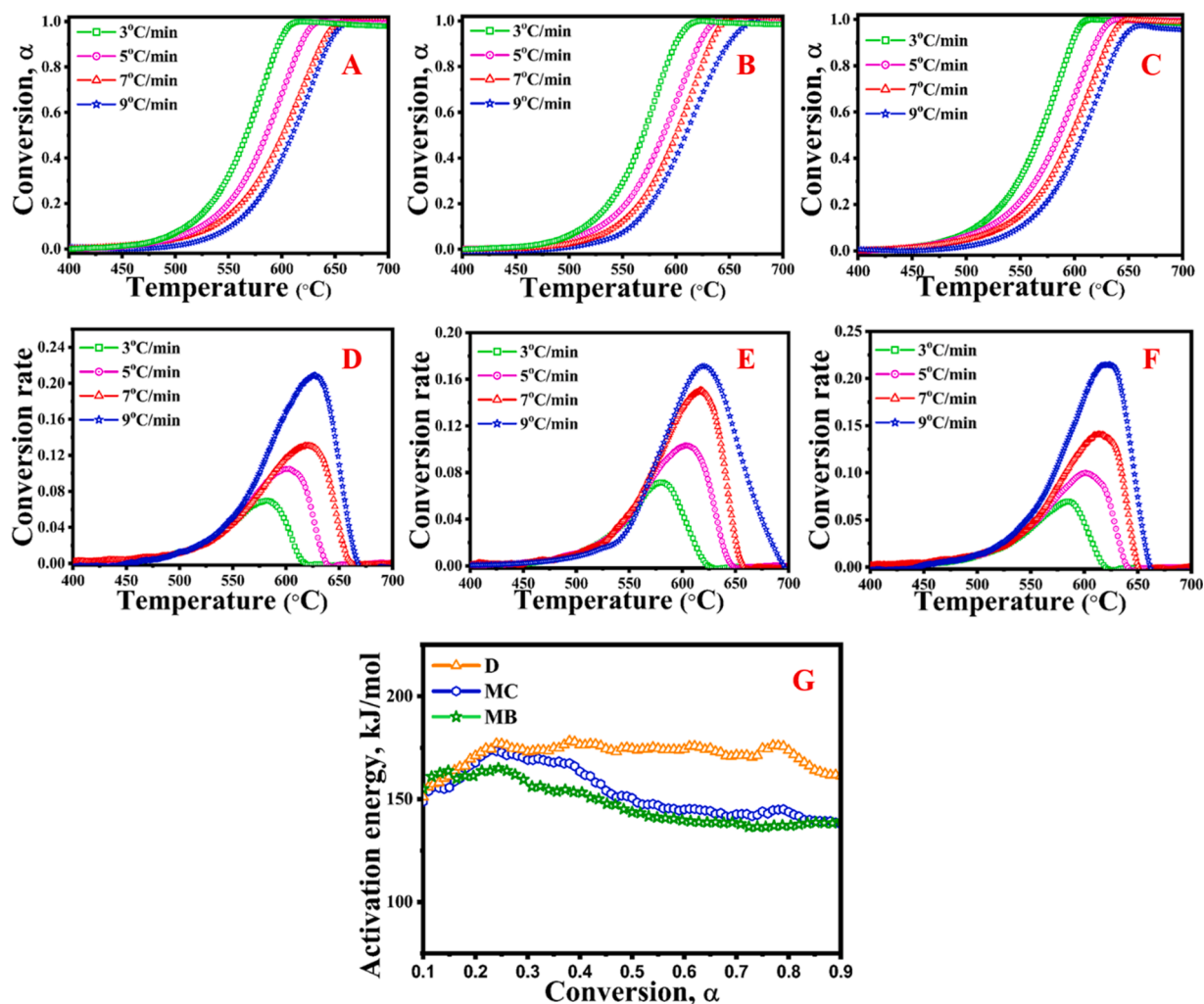


Fig. 2. Soot conversion, α , for (A) MBD-25 (B) MCD-25 and (C) D; soot conversion rate ($d\alpha/dt$) measured in air at different heating rates for (D) MBD-25 (E) MCD-25 and (F) D. Variation in the activation energy at different soot conversion levels (G).

are largely similar. This can be attributed to the oxidation of disordered regions of the soot predominantly at the core end of the particles. Progression towards higher conversion levels expresses an increase in activation energy for D, which could be credited to a relative decrease in the number of oxygen functionalities on the soot surface. Man et al. [50] proposed that the higher oxygen content in soot results in an increase in the evaporation rate of loosely bound volatile materials and induces internal oxidation in the soot structure [50]. Furthermore, higher activation energies and high temperatures are needed for oxidation of graphitized peripheral regions of the soot. The activation energy is the highest for D, followed by MCD-25 and MBD-25 throughout the conversion levels. The estimated values of the mean activation energies at all conversion levels were 155.4, 165.0, and 175.1 kJ/mol for MBD-25, MCD-25, and D, respectively. This suggests that greater degree of graphitization is present in diesel soot which reduces due to enhanced internal soot oxidation with the addition of surrogate fuels to diesel. Literature suggests that the activation energies for soot and carbon samples are located in the range of 130–200 kJ/mol, which agrees with the acquired data [51]. Oxygen-rich fuel systems have been reported to enhance the decomposition of solid bound oxygen functional groups to form CO and CO₂. As will be discussed in the subsequent elemental analysis section, higher oxygen content results in the greater vulnerability of carbon atoms to undergo oxidation, thereby spurring up the oxidation rate, which is in accord with the activation energy values obtained from TGA analysis. [52] Moreover, the cooperation of a wide

number of parameters such as crystallinity, structural irregularity, tortuosity, fringe length, etc., together develop into enhancing the soot oxidation kinetics. Hence, the soot samples were subjected to HRTEM, EDX, XRD, Raman, and Surface area measurements to better understand these effects [53–55].

3.3. High resolution transmission electron microscopy (HRTEM)

Fig. 3 exhibits the quintessential HRTEM images of the soot samples derived from the flame setup for diesel, MBD-25, and MCD-25. For enhanced reliability of the analysis, a sampling region with a higher concentration of soot particles was identified under low magnification i. e., 100, 50 nm and this was followed by higher-magnification (500 KX), high-resolution imaging (5 nm) to observe the soot core-shell structure. For consistency in image analysis, the imaging has been carried out in three-folds for each representative soot sample. Fringe length and tortuosity has been calculated using these microstructural images of each primary particle, having at least >1300 fringe microstructures. The soot samples resemble an agglomerated and welded rather spherical carbon spherules. The merging of primary soot particles with neighbouring particles is partly due to chain growth and somewhat an effect of sintering. Although the particles appear fairly soldered together in the forms of chains and branches having a grid-like framework, the branch and chain endings allow individual spherules to be analysed. The primary soot particles display an amorphous, disordered core structure,

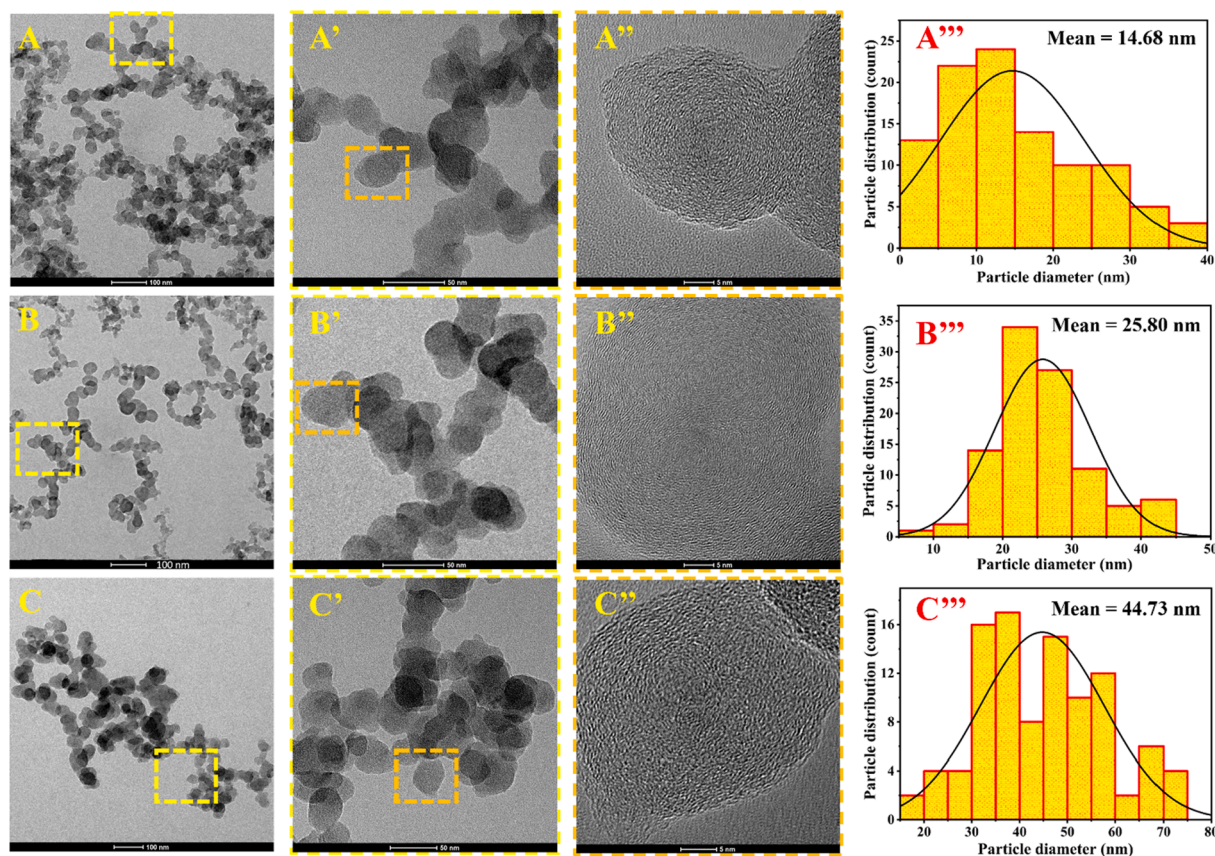


Fig. 3. TEM images of samples developed at low (100 nm and 50 nm) and high (5 nm) magnification. The images portray the primary soot particle size distribution (± 5 nm) of (A, A', A'', A''') MBD-25 soot, (B, B', B'', B''') MCD-25 soot, and (C, C', C'', C''') D soot.

and the outer shell is composed of graphitic layers with curved fringes of reasonable order. The investigation of nearly 100 primary soot particles for size distribution was performed using ImageJ software. The nature of this distribution was analysed using Microsoft excel to identify kurtosis and skewness values. The calculated values of kurtosis and skewness are in the range of -0.4 to $+0.4$ and -0.08 to 0.5 respectively which illustrates approximate symmetry and is close to the normal distribution [56].

MBD and MCD being oxygenated fuels, are known to bring about enhanced combustion efficiency and decrease pollutant emissions due to the presence of internal fuel oxygen [12]. The existence of this oxygen bound to the fuel, lowers down the soot production [57]. Due to this internal oxygen, the soot oxidation kinetics surpasses the soot formation kinetics, consequently resulting in reduced size of soot particles [58]. The mean particle diameters of MBD-25, MCD-25, and D are 14.68, 25.80, and 44.73 respectively. Fig. 3 is in accordance with the fact that the soot formed on the addition of surrogate fuels has diminished order and is additionally oxidized compared to the soot produced by pure diesel. The blending of the biofuel surrogates with diesel results in a decreased diameter of soot particles consistent with the observations of Das et al. [57]. This observation is in accordance with the mean particle values calculated in this study [57]. The presence of oxygen in the soot particles was confirmed from the EDX data which will be presented in the subsequent section. From Fig. 3 it can be noted that there is a measurable difference between the soot particle size of MBD-25 and MCD-25. This difference could be attributed to the presence of unsaturated C=C bond in MCD. The unsaturation points towards several variations in the physical, chemical, and structural properties, which eventually initiates differences in combustion performances of the two biofuel surrogates. The initial oxidation steps are rather similar for both the surrogates but in case of MCD, the unsaturation in conjugation with

C=O functional group could initiate the formation of resonance stabilized radicals as reported by Arkke et al. [59,60]. Subsequently, this facilitates formation of cyclic PAH nuclei thus increasing the number of soot precursor and dominant growth of soot particles to a bigger size as compared to MBD soot.

The fringe length and fringe tortuosity were analysed quantitatively using a MATLAB algorithm constructed concerning a set of codes and equations specified by Yehliu et al. [61,62] This investigation is constituted of two main parts i.e., digital image processing and lattice fringe characterization. The individual HRTEM micrographs were subjected to greyscale conversion and negative transformation expressed as $I_{negative} = L - I_{original}$, where $I_{original}$ is the image pixel value (round about 256 per image) before transformation and L is the discrete intensity levels. The regions of interest (ROI) were selected, and procedures such as contrast enhancement, Gaussian lowpass filter, and top-hat transformation were implemented, which aid in refining the fringe contrast throughout the image and also excludes errors due to non-homogeneous illumination, which subsequently intensify the fringe contrast. From each of the TEM images with more than 100 distinguishable soot particles, four microstructural high-resolution images of primary particles were chosen indiscriminately, having a minimal of >1300 fringe microstructures. The fringe structure analysis using MATLAB specifies the mean values of the fringe length and fringe tortuosity. A built-in function in MATLAB known as “branchpoints” that employs a parallel thinning algorithm is used to remove branches from fringes. The analysis of the fringe patterns obtained from the above analysis is presented in Table 2, and the fringe structures are exemplified in Fig. 4.

The MBD-25 and MCD-25 soot samples represent a somewhat irregular onion-like structure and display a higher degree of fringe curvature and longer fringe lengths in contrast to diesel soot. Some of the fringes appear almost parallel, while others are randomly oriented.

Table 2
Summary of calculated soot nanocrystallite parameters.

Properties	Soot Samples		
	MBD-25	MCD-25	D
XRD Results			
Interlayer spacing, d002	0.389 nm	0.386 nm	0.366 nm
Nanocrystallite height, L_c	1.054 ± 0.5 nm	0.957 ± 0.5 nm	1.030 ± 0.5 nm
Nanocrystallite width, L_a	3.640 ± 0.5 nm	3.560 ± 0.5 nm	3.500 ± 0.5 nm
HRTEM Results			
Mean fringe length	2.25 nm	2.10 nm	1.52 nm
Mean fringe tortuosity	1.72	1.61	1.58
Mean primary particle diameter	14.68 ± 5 nm	25.80 ± 5 nm	44.73 ± 5 nm
Raman Results			
I_{D1}/I_G	1.36	1.30	1.13
Lattice width, L_c	3.23 nm	3.37 nm	3.88 nm

As elucidated by Lapuerta et al. [63], the curvature of the graphene layers i.e., the tortuosity can be correlated with the degree of order in the soot nanostructure, the authors suggested that it can be well expected that the soot reactivity and consequently its oxidation increases as the nanostructural order decreases [63]. Enhanced soot oxidation as observed in TGA is a result of greater fringe tortuosity especially at mid conversion levels. The increase in tortuosity values are associated with

the formation of five-membered ring structures that increases disorder in the six membered graphitic carbon structure of soot. A confirmation of this effect can also be observed from the work of Abdrabou et al. [3] wherein deliberate addition of 5-membered bicyclic oxygenated additives were found to significantly increase tortuosity in the diesel combustion derived soot. The values presented in Table 2 reveal that pure diesel has the lowest fringe tortuosity indicating poor soot oxidation properties. The surrogate blend MCD-25 shows lower fringe tortuosity compared to the methyl butyrate diesel blend, justifying the observed trend of soot reactivity in TGA analysis. The mean fringe length is the lowest for D (1.52) and increases for MCD-25 (2.10) followed by MBD-25 (2.25). These features together indicate that MBD-25 displays greater disorder and hence is subjected to greater oxidation. This characteristic is highly desirable in automobiles for faster regeneration of diesel particulate filters.

3.4. X-ray diffraction

The soot produced from D, MBD-25, and MCD-25 was subjected to X-ray diffraction analysis. The quantitative information concerning the PAH stacking, interplanar separation etc. can be obtained from the XRD plot. As seen in Fig. 5, two broadened, low-intensity peaks are obtained at 24° and 44° . The interlayer spacing and thickness of the PAH stack can be found using the 1st peak at 24° , assigned as the (002) plane. Likewise, the average size of the PAH's in soot can be found using the 2nd

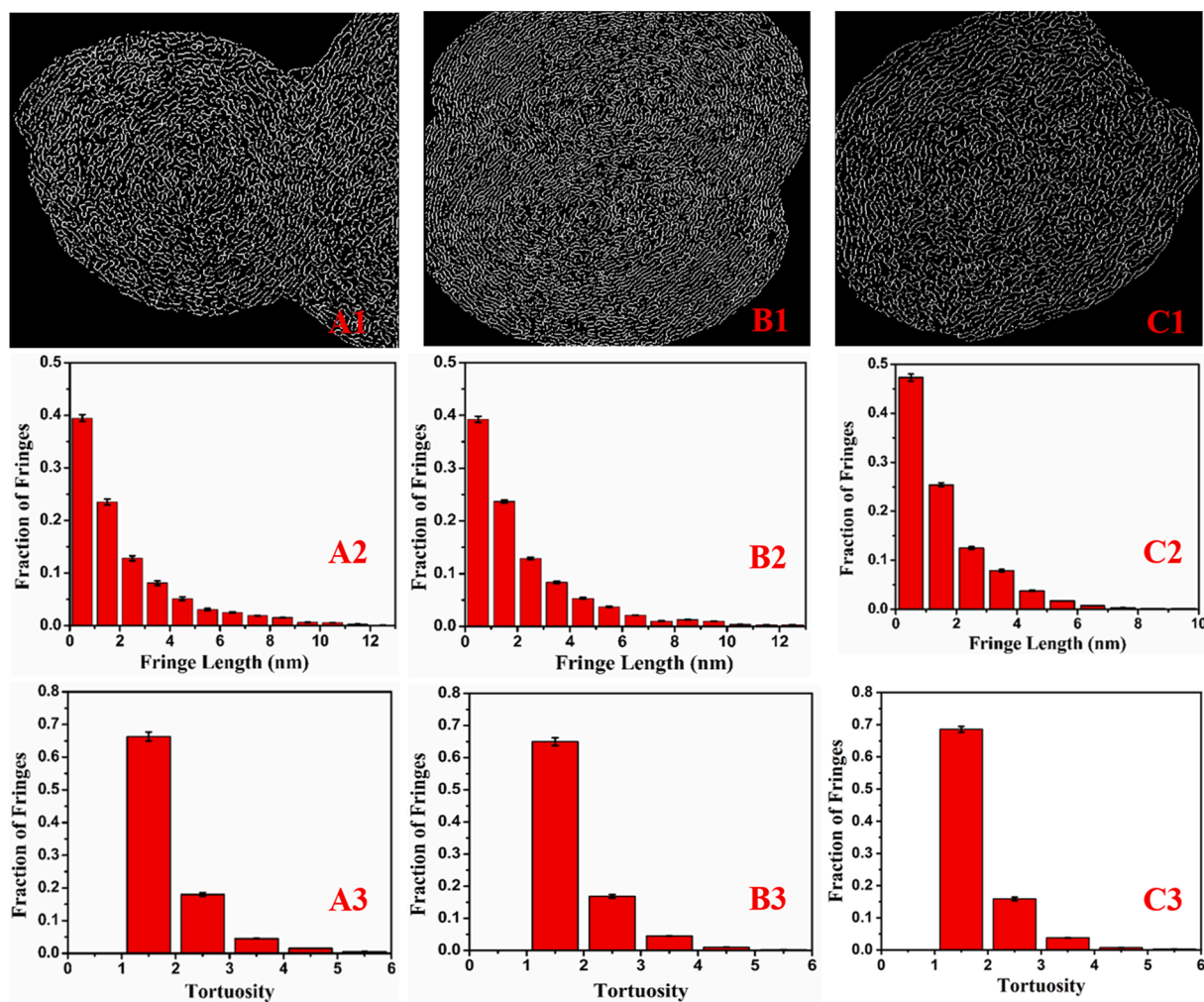


Fig. 4. MATLAB processed fringe nanostructure i.e. fringe length and fringe tortuosity distribution of (i) MBD-25 (A1, A2, A3), (ii) MCD-25 (B1, B2, B3), and (iii) D (C1, C2, C3) soots obtained from analysis of corresponding HRTEM images A", B" and C" from Fig. 3. Bin width is fixed to 1 for better comparison of the three soot samples.

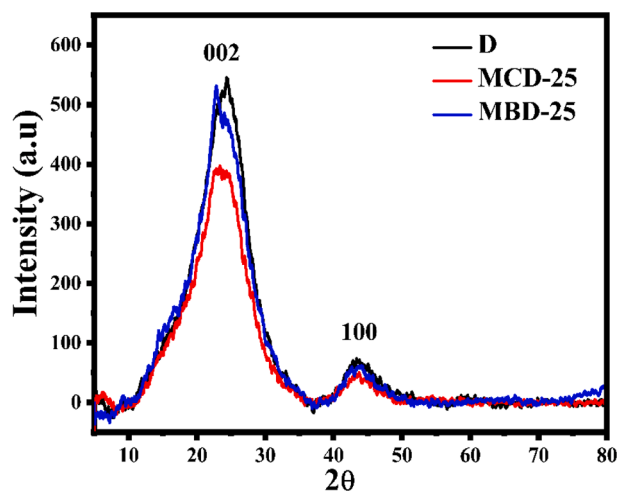


Fig. 5. XRD pattern of soot samples derived from MBD-25, MCD-25, and D.

peak observed at 44°, designated to the (1 0 0) plane. As given by Bragg's law stated in equation (4), the interlayer PAH spacing of d_{002} can be determined. The width of the nanocrystallite (L_a), which furnishes the average size of the PAH stack, can be computed using the Scherrer formula given in equation (5). The height of the nanocrystallite (L_c), which assigns the thickness of the PAH stack, can be determined using the formula given in equation (6).

$$d_{002} = \frac{\lambda}{2\sin\theta_{002}} \quad (4)$$

$$L_a = \frac{0.9\lambda}{\beta_{002}\cos\theta_{002}} \quad (5)$$

$$L_c = \frac{1.84\lambda}{\beta_{002}\cos\theta_{100}} \quad (6)$$

In the above equations, k denotes the shape factor which is set as 0.9 for spherical particles, λ is the wavelength of X-ray (0.54 nm for Cu $K\alpha$), β_{002} and β_{100} are attested to the full width at half maximum (FWHM) for the two peaks and θ_{002} and θ_{001} are the Bragg's angles. Gaussian fitting of the characteristic peaks was carried out using MATLAB software to establish Bragg's angles and the FWHM. The interlayer separation between the graphitic planes is higher in MBD-25 and MCD-25 in comparison to diesel by a factor of 0.023 and 0.020 respectively [9,10,64] which can facilitate greater diffusion of O_2 through the disordered structure and hence greater oxidative reactivity as observed in TGA. The L_a and L_c values are almost similar for all three soot samples and the difference could not be accurately quantified using a bulk sample analysis via XRD. Nonetheless, further evidence of the crystal structure disorder and better estimation of L_a values were achieved from the Raman analysis, these results are discussed in the next section.

3.5. Raman analysis

The Raman spectrum observed in the region of 800–1800 cm^{-1} shows two characteristic bands at around 1350 and 1590 cm^{-1}

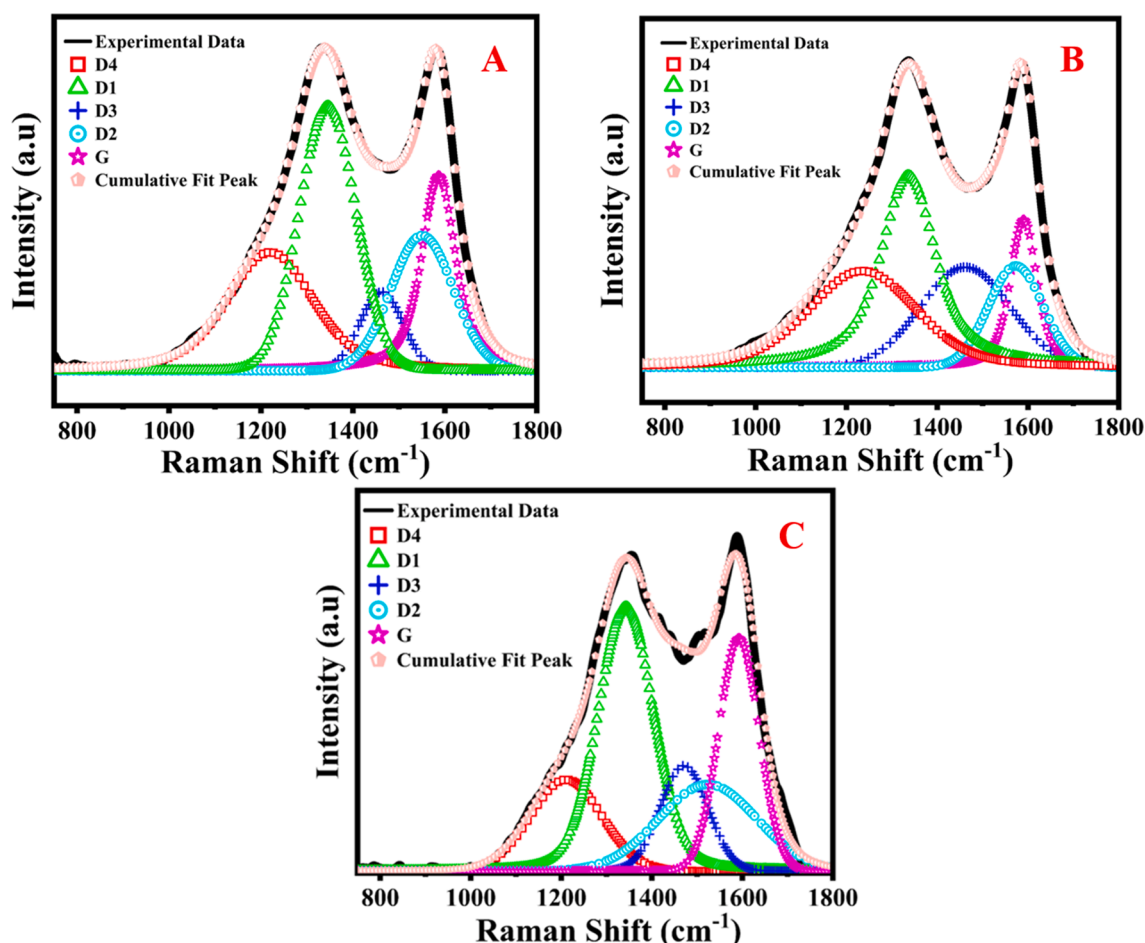


Fig. 6. Raman spectra of (A) MBD-25, (B) MCD-25, and (C) D.

analogous to the D and G band, respectively (see Fig. 6). This spectroscopic technique characterizes the internal structure of carbonaceous materials, and unlike XRD studies, it not only provides data regarding the crystallinity of a substance but also provides an understanding of the amorphous carbon content in soot. The D band corresponds to the disordered structure and is related to the aliphatic content of the soot particles, and the G band denotes the graphitic structure observed along the outer shell structure of the soot particles. A five curve deconvolution model was used to analyse the Raman spectra, wherein the raw data were fitted using the Voight peak fitting function as suggested by Catalani et al. [65]. The five fitted peaks are D1, D2, D3, D4, and G, where D1 is the most intense suggesting the lattice disorder. The D2 band indicates lattice vibrations, and D3 and D4 correspondingly indicate amorphous carbon linked to organic molecules and carbon-carbon stretching frequencies. The ratio of the relative intensities of the D band and G band is associated with the structural defects and indicates the degree of disorientation in the basal plane of the graphitic layers [66,67].

The ratio of I_D/I_G can be related to the lattice width (L_a) using the Knight and White equation (equation (7)) as suggested by Escribano et al. [68]. For an excitation wavelength of 532 nm, a proportionality constant of 4.4 is used as specified by Raj et al. [69,70].

$$L_a = 4.4 \left(\frac{I_{D1}}{I_G} \right)^{-1} \quad (7)$$

The I_{D1}/I_G values of D and the blends are stated in Table 2, along with the analogous values of L_a . The value of I_{D1}/I_G is highest for MBD-25, followed by MCD-25 and D, and the consequent values of L_a decrease in moving from D to MBD-25. The values of L_a suggest that the lattice disorder intensifies on blending of diesel with the surrogate fuels. The overall results obtained in this study are comparable to the results obtained by Jiang et al. [12]. The study based on surrogate fuels using an ethylene inverse diffusion flame concluded that the MB fuel indicated greater soot disorder in comparison to the MC fuel [12]. The results obtained in this study from HRTEM analysis also suggests a similar trend as above which agrees well with the work of Jiang et al. [12]. Thus among the 2 surrogate fuels under study having similar structural characteristics, the saturated variant has been found to enhance soot oxidation kinetics more than the unsaturated variant.

This trend is in agreement with the HRTEM, and TGA studies, wherein MBD-25 exhibited the smallest particle size, highest tortuosity, crystal structure disorder and enhanced reactivity compared to the rest of the soot samples. Furthermore, the influence of fuel-bound oxygen on soot's oxygen content was investigated using EDX and CHNS analyser, the results of which are presented in the next section [71].

3.6. Elemental analysis (CHNS and EDX)

Morajkar et al. [9] has previously reported that the percentage of oxygen functional groups in fuel additives, specifically biofuels, trigger higher percentages of oxygen in the soot samples. This consequently leads to an intensification in the rate of soot oxidation kinetics [9]. Since both the biodiesel surrogate fuels used in this study comprise of a fuel bound oxygen atom, it is essential to measure the comparative C/O ratio in soot samples collected from pure diesel and the MBD-25 and MCD-25 blends. The estimation of this proportion was carried out independently

using a calibrated CHNS analyser and an Energy Dispersive X-ray Spectra (EDX) analyser. The data obtained from EDX was processed using the eZAF Smart Quant analyser. The results are together expressed in Table 3 and the figures expressing the elemental composition obtained from EDX is presented in the supplementary fig. S4. For the CHNS analysis, three samples were analysed and the means were reported. For EDX analysis, the weight and atomic percentages of carbon and oxygen were measured for each sample in two different regions (A1-A2). It's apparent that the soot samples obtained from blended fuels have a higher oxygen content as compared to pure diesel. Since the presence of oxygen was confirmed through EDX analysis, the % O was calculated from the CHNS data as shown in Table 3. This allowed a comparison of the C/O ratios obtained from both the analysis methods. The trend of C/O ratio obtained from the two different methods confirm that the % of O is significantly higher in case of surrogate blended diesel soot as compared to pure diesel soot. Thus confirming that oxygenated fuels do produce highly oxygenated soot which further facilitates its greater reactivity and enhanced internal oxidation of the soot as observed in TG studies. A comparison of the two surrogate blended diesel soot reveal that not a significant difference in oxygen content exists between the two soot. Hence the observed difference in the oxidative reactivity between MBD-25 and MCD-25 is a result of the significant difference in the particle size and greater crystal structure disorder in the former case. Since soot surface area is another important factor that could facilitate oxidative reactivity of the soot, BET N_2 isotherm analysis were performed, results of which are discussed in the next section.

3.7. BET surface area analysis

The surface area plays a vital role in reactions involving both solids and gases. The greater surface area of soot particles results in greater O_2 adsorption as well as diffusion access through the internal structure of the soot. This could augment soot reactivity significantly [72]. Therefore, the total surface area of the soot samples was evaluated using the BET N_2 adsorption-desorption isotherm studies [63].

As shown in Fig. 7, all soot samples display Type II isotherm with no hysteresis loop confirming that, the soot samples are non-porous in nature with unrestricted monolayer-multilayer adsorption access. Total surface area analysis gave values of 91.0, 82.7 and 78.5 (± 1) m^2/g in case of MBD-25, MCD-25 and D soot respectively. This result confirmed that the blending of surrogates especially MB with diesel enhances the surface area of the soot. This could well be attributed to the greater degree of oxidation of the MBD-25 soot, leading to smaller particle size, and greater lattice disorder as observed in HRTEM and Raman analysis. Therefore, all the above factors together contribute towards greater oxidative reactivity of MBD-25 soot in comparison to the rest of the samples.

3.8. Implications of structural differences in MB and MC on soot oxidation kinetics

Although similar in structure, the presence of unsaturation and saturation in MC and MB respectively results in quiet a difference in the soot nanostructure and oxidative reactivity. Comparing the two blends, the soot formation and oxidation rate of MCD-25 is greater compared to MBD-25 by a factor of 1.41 and 1.06 respectively. Furthermore, the nanostructural characterization of the blends revealed enhanced

Table 3
Elemental composition of MBD-25, MCD-25, and D.

CHNS Analysis						EDX Analysis			
Sample	C [%]	H [%]	N [%]	S [%]	$O_{calc.} (100-C\%+H\%+N\%+S\%)$	$C/O_{calc.}$	C [%]	O [%]	C/O
MBD-25	94.08	1.62	0.06	0.00	4.23	22.24	91.71	8.29	11.06
MCD-25	94.62	1.41	0.04	0.00	3.93	24.08	92.98	7.02	13.25
D	94.64	1.71	0.05	0.00	3.60	26.29	95.34	4.66	20.41

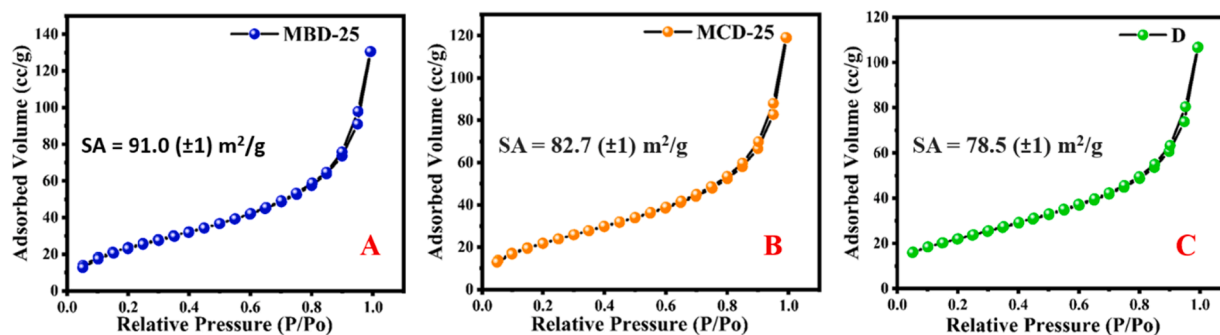
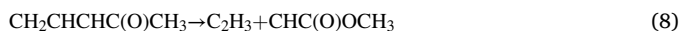


Fig. 7. Nitrogen adsorption–desorption isotherms of the (A) MBD-25, (B) MCD-25, and (C) D soot samples.

disorder, higher fringe tortuosity, greater interlayer spacing and smallest mean particle diameter for MBD-25 in comparison to MCD-25. This difference could arise due to a difference in the pyrolysis pathway generating different radicals and their subsequent reactions with O_2 . As discussed earlier, the RSR's have been found to play a significant role in gas-phase kinetics especially in the case of MCD-25. The existence of RSR's has been confirmed through the works of Joshi et al. [59] using a photo-ionization-mass-spectrometer. These RSR's have been also reported to significantly alter the autoignition characteristics in shock tubes experiments and kinetic modelling studies of Vallabhuni et al. [24], though they did not study its influence of soot formation kinetics.

A collective analysis of the reported RSR's chemistry of MC and all the results obtained in this study of MCD-25 in comparison to MBD-25 clearly suggests that, these RSR's do have an influence on soot formation and its oxidation kinetics. This can be attributed to the fact that, due to unsaturation in MC, the rate of H-abstraction reactions which govern the initial fuel oxidation rates would be significantly different in MC and MB [73]. MC has three allylic H atoms which can be easily abstracted and is a predominant reaction pathway as contemplated by Zhou et al. [74]. Consequently, the immediate radicals formed are of the type $CH_2CHCHC(O)OCH_3$, $CH_3CCHC(O)OCH_3$, $CH_3CHCC(O)OCH_3$, and $CH_3CHCHC(O)OCH_2$. Out of these, $CH_2CHCHC(O)OCH_3$ is formed due to allylic H-abstraction and is a highly resonance stabilised structure. It has been also suggested by Joshi et al. [59] that the bimolecular reaction with molecular oxygen of this radical is quite slow [42,59,75]. On the contrary, MB oxidation through H-abstraction produces $CH_2CH_2CH_2C(O)OCH_3$ radicals, which reacts with a relatively lower activation energy with O_2 in comparison to the MC radical. These differences in their reactivities could govern the observed trends in sooting propensities of the blends in flame [14,60,76]. The predominant radicals formed decompose to form C_2H_3 via the following reaction [14],



Subsequently, C_2H_3 radicals transform into propargyl (C_3H_3) radicals, which combine via a complex multiphase chemistry to produce unsaturated PAH nuclei's which serve as precursors for soot formation [77]. The low reactivity of $CH_2CHCHC(O)OCH_3$ radicals with oxygen, could therefore favour the soot production rate in MCD-25 unlike MBD-25. Consequently, this leads to greater soot particle size and lower nanostructural disorder in MCD. These properties lead to the proposition that the oxidation of soot particles obtained is in the trend, MBD-25 > MCD-25 > D.

4. Conclusion

The effect of blending the two surrogate fuels MB and MC with diesel on sooting propensity of the blends and subsequently on the nanostructure and reactivity of the soot samples were investigated. The physicochemical features aided in distinguishing the properties associated with the fuel blends. The calorific values obtained are in agreement with the higher oxygen content of the fuel blends compared to pure

diesel. The smoke point studies suggested that the 25% blend was the optimal one for both fuels, considerably reducing soot formation rate of diesel fuel. The characterization of the soot particles through HRTEM, XRD, Raman, and elemental studies confirmed that the MBD-25 soot has a smaller primary particle size, higher tortuosity, greater interlayer spacing, and structural disorder as compared to the MCD-25 and pure diesel soot. These characteristics result in enhanced oxidative reactivity in MBD-25 compared to the rest of the fuels under investigation. The striking difference in the soot production rate, nanostructural characteristics and oxidative reactivity between MCD-25 and MBD-25 is attributed to the fact that, the radicals produced in MCD-25 combustion exhibit resonance stabilization effect due to the presence of a double bond in conjugation with the ester carbonyl group. This probably resulted in its lower reactivity with O_2 in flame and hence has a significant effect on soot characteristics and subsequently on its oxidative reactivity. Therefore, this study suggests that the resonance stabilization effects do influence the soot formation and oxidation kinetics and hence should be taken into account while constructing global multiphase predictive kinetic models of biodiesel combustion.

CRediT authorship contribution statement

Samantha Da Costa: Data curation, Formal analysis, Writing – original draft. **Akshay Salkar:** Data curation, Formal analysis, Writing – original draft. **Anand Krishnasamy:** Formal analysis, Visualization. **Ravi Fernandes:** Visualization, Formal analysis, Software. **Pranay Morajkar:** Conceptualization, Supervision, Funding acquisition, Methodology, Resources, Validation, Visualization, Writing - review & editing.

Declaration of Competing Interest

The authors declare that they have no known competing financial interests or personal relationships that could have appeared to influence the work reported in this paper.

Acknowledgements

The authors acknowledge the following funding agencies for the financial support provided by the DST, India through the DST/INNO-INDIGO (DST/IMRCD/INNO-INDIGO/BIOCFD/2017(G)) and DST SERB (ECR/2015/000047). The authors also acknowledge UGC, New Delhi, at the level of DSA-I under the Special Assistance Program (SAP) (F. No. 540/14/DSA-I/2015/(SAP-I)). The authors acknowledge SAIIF, IITB for providing HRTEM analysis. Mr. Akshay V. Salkar acknowledges DST, New Delhi for providing research fellowship.

Appendix A. Supplementary data

Supplementary data to this article can be found online at <https://doi.org/10.1016/j.fuel.2021.122141>.

References

- [1] Islam N, Dihingia A, Khare P, Saikia BK. Atmospheric particulate matters in an Indian urban area: health implications from potentially hazardous elements, cytotoxicity, and genotoxicity studies. *J Hazard Mater* 2020;384:121472. <https://doi.org/10.1016/j.jhazmat.2019.121472>.
- [2] Guerrero Peña GDJ, Hammid YA, Raj A, Stephen S, Anjana T, Balasubramanian V. On the characteristics and reactivity of soot particles from ethanol-gasoline and 2,5-dimethylfuran-gasoline blends. *Fuel* 2018;222:42–55. <https://doi.org/10.1016/j.fuel.2018.02.147>.
- [3] Abdrabou MK, Morajkar PP, Guerrero Peña GDJ, Raj A, Elkadi M, Salkar AV. Effect of 5-membered bicyclic hydrocarbon additives on nanostructural disorder and oxidative reactivity of diffusion flame-generated diesel soot. *Fuel* 2020;275:117918. <https://doi.org/10.1016/j.fuel.2020.117918>.
- [4] Alrefaai MM, Guerrero Peña GDJ, Raj A, Stephen S, Anjana T, Dindi A. Impact of dicyclopentadiene addition to diesel on cetane number, sooting propensity, and soot characteristics. *Fuel* 2018;216:110–20. <https://doi.org/10.1016/j.fuel.2017.11.145>.
- [5] Imtenan S, Varman M, Masjuki HH, Kalam MA, Sajjad H, Arbab MI, et al. Impact of low temperature combustion attaining strategies on diesel engine emissions for diesel and biodiesels: a review. *Energy Convers Manag* 2014;80:329–56. <https://doi.org/10.1016/j.enconman.2014.01.020>.
- [6] Krishnasamy A, Gupta SK, Reitz RD. Prospective fuels for diesel low temperature combustion engine applications: a critical review. *Int J Engine Res*. SAGE Publications Ltd September 30, 2020. 10.1177/1468087420960857.
- [7] Krishnamoorthi M, Malayalamurthi R, He Z, Kandasamy S. A review on low temperature combustion engines: performance, combustion and emission characteristics. *Renew Sustain Energy Rev Elsevier Ltd* 2019;116:109404. <https://doi.org/10.1016/j.rser.2019.109404>.
- [8] Morajkar PP, Abdrabou MK, Raj A, Elkadi M, Stephen S, Ibrahim Ali M. Transmission of trace metals from fuels to soot particles: an icp-ms and soot nanostructural disorder study using diesel and diesel/Karanja biodiesel blend. *Fuel* 2020;280:118631. <https://doi.org/10.1016/j.fuel.2020.118631>.
- [9] Morajkar PP, Guerrero Peña GDJ, Raj A, Elkadi M, Rahman RK, Salkar AV, et al. Effects of camphor oil addition to diesel on the nanostructures and oxidative reactivity of combustion-generated soot. *Energy Fuels* 2019;33(12):12852–64. <https://doi.org/10.1021/acs.energyfuels.9b03390>.
- [10] Morajkar PP, Abdrabou MK, Salkar AV, Raj A, Elkadi M, Anjum DH. Nanostructural disorder and reactivity comparison of flame soot and engine soot using diesel and jatropa biodiesel/diesel blend as fuels. *Energy Fuels* 2020;34(10):12960–71. <https://doi.org/10.1021/acs.energyfuels.0c02063>.
- [11] Liu D, Wang Y, Ying Y, Luo M. Nanostructure and reactivity of carbon particles from co-pyrolysis of biodiesel surrogate methyl octanoate blended with *n*-butanol. *Fullerenes Nanotub Carbon Nanostructures* 2018;26(5):278–90. <https://doi.org/10.1080/1536383X.2018.1436052>.
- [12] Jiang B, Liu D, Lin Z. Soot particles diagnostics in ethylene inverse diffusion flame blending with biodiesel surrogates of saturated methyl butyrate and unsaturated methyl crotonate. *Fuel Process Technol* 2020;202:106379. <https://doi.org/10.1016/j.fuproc.2020.106379>.
- [13] Schönborn A, Ladommatos N, Williams J, Allan R, Rogerson J. The influence of molecular structure of fatty acid monoalkyl esters on diesel combustion. *Combust Flame* 2009;156(7):1396–412. <https://doi.org/10.1016/j.combustflame.2009.03.011>.
- [14] Gao Z, Zhu L, Liu C, Li A, He Z, Zhang C, et al. Comparison of soot formation, evolution, and oxidation reactivity of two biodiesel surrogates. *Energy Fuels* 2017;31(8):8655–64. <https://doi.org/10.1021/acs.energyfuels.7b00922>.
- [15] Zannis TC, Hountalas DT, Kouremenos DA. Experimental investigation to specify the effect of oxygenated additive content and type on DI diesel engine performance and emissions. *SAE Tech Pap* 2004. <https://doi.org/10.4271/2004-01-0097>.
- [16] Pepiot-Desjardins P, Pitsch H, Malhotra R, Kirby SR, Boehman AL. Structural group analysis for soot reduction tendency of oxygenated fuels. *Combust Flame* 2008;154(1–2):191–205. <https://doi.org/10.1016/J.COMBUSTFLAME.2008.03.017>.
- [17] Baskar P, Senthilkumar A. Effects of oxygen enriched combustion on pollution and performance characteristics of a diesel engine. *Eng Sci Technol Int J* 2016;19(1):438–43. <https://doi.org/10.1016/J.JESTCH.2015.08.011>.
- [18] Palazzo N, Zigan L, Huber FJT, Will S. Impact of oxygenated additives on soot properties during diesel combustion. *Energies* 2021;14(1):147. <https://doi.org/10.3390/en14010147>.
- [19] Liu H, Bi X, Huo M, Lee CFF, Yao M. Soot emissions of various oxygenated biofuels in conventional diesel combustion and low-temperature combustion conditions. *Energy Fuels* 2012;26(3):1900–11. <https://doi.org/10.1021/ef201720d>.
- [20] Iida N, Suzuki Y, Sato GT, Sawada T. Effects of intake oxygen concentration on the characteristics of particulate emissions from a D.I. diesel engine. *SAE Tech Pap* 1986. <https://doi.org/10.4271/861233>.
- [21] Verma P, Jafari M, Rahmani SMA, Pickering E, Stevanovic S, Dowell A, et al. The impact of chemical composition of oxygenated fuels on morphology and nanostructure of soot particles. *Fuel* 2020;259:116167. <https://doi.org/10.1016/j.fuel.2019.116167>.
- [22] Kholghy MR, Weingarten J, Sediako AD, Barba J, Lapuerta M, Thomson MJ. Structural effects of biodiesel on soot formation in a laminar coflow diffusion flame. *Proc Combust Inst* 2017;36(1):1321–8. <https://doi.org/10.1016/j.proci.2016.06.119>.
- [23] Lele AD, Vallabhuni SK, Moshhammer K, Fernandes RX, Krishnasamy A, Narayanaswamy K. Experimental and chemical kinetic modeling investigation of methyl butanoate as a component of biodiesel surrogate. *Combust Flame* 2018;197:49–64. <https://doi.org/10.1016/J.COMBUSTFLAME.2018.06.033>.
- [24] Vallabhuni SK, Johnson PN, Shu B, Narayanaswamy K, Fernandes RX. Experimental and kinetic modeling studies on the auto-ignition of methyl crotonate at high pressures and intermediate temperatures. *Proc Combust Inst* 2020;38(1):223–31. <https://doi.org/10.1016/j.proci.2020.06.083>.
- [25] Rodenbush CM, Hsieh FH, Viswanath DS. Density and viscosity of vegetable oils. *J Am Oil Chem Soc* 1999;76(12):1415–9. <https://doi.org/10.1007/s11746-999-0177-1>.
- [26] Esteban B, Riba JR, Baquero G, Rius A, Puig R. Temperature dependence of density and viscosity of vegetable oils. *Biomass Bioenergy* 2012;42:164–71. <https://doi.org/10.1016/j.biombioe.2012.03.007>.
- [27] Liang F, Lu M, Keener TC, Liu Z, Khang SJ. The organic composition of diesel particulate matter, diesel fuel and engine oil of a non-road diesel generator. *J Environ Monit* 2005;7(10):983–8. <https://doi.org/10.1039/b504728e>.
- [28] Glassman, Yaccarino, P. The effect of oxygen concentration on sooting diffusion flames. <https://doi.org/10.1080/00102208008952429> 2007, 24 (3–4), 107–114. 10.1080/00102208008952429.
- [29] Watson RJ, Botero ML, Ness CJ, Morgan NM, Kraft M. An improved methodology for determining threshold sooting indices from smoke point lamps. *Fuel* 2013;111:120–30. <https://doi.org/10.1016/J.FUEL.2013.04.024>.
- [30] Jha SK, Fernando S, To SDF. Flame temperature analysis of biodiesel blends and components. *Fuel* 2008;87(10–11):1982–8. <https://doi.org/10.1016/J.FUEL.2007.10.026>.
- [31] Merchan-Merchan W, Granados Sanmiguel S, McCollam S. Analysis of soot particles derived from biodiesels and diesel fuel air-flames. *Fuel* 2012;102:525–35. <https://doi.org/10.1016/J.FUEL.2012.04.029>.
- [32] Patnaik P, Dean JA. (John A. Dean's Analytical Chemistry Handbook. 2004.
- [33] Hernández-Giménez AM, Castelló DL, Bueno-López A. Diesel Soot combustion catalysts: review of active phases. *Chem Pap Versita* 2014;1154–68. <https://doi.org/10.2478/s11696-013-0469-7>.
- [34] Atabani AE, César ADS. Calophyllum Inophyllum L. - A prospective non-edible biodiesel feedstock. study of biodiesel production, properties, fatty acid composition, blending and engine performance. *Renewable Sustain Energy Rev*. Elsevier Ltd 2014, pp 644–655. 10.1016/j.rser.2014.05.037.
- [35] Kaisan MU, Anafi FO, Nuszowski J, Kulla DM, Umaru S. Calorific value, flash point and cetane number of biodiesel from cotton, jatropa and neem binary and multi-blends with diesel. *Biofuels* 2020;11(3):321–7. <https://doi.org/10.1080/17597269.2017.1358944>.
- [36] Rena, Gautam P, Kumar S. Landfill gas as an energy source. In *Current developments in biotechnology and bioengineering: waste treatment processes for energy generation*; Elsevier, 2019; pp 93–117. 10.1016/B978-0-444-64083-3.00006-3.
- [37] Hussain A, Mehdi SM, Akhtar M, Ani FN, Ahmed I. Combustion performance of diesel palm olein fuel: a combined CFD and experimental approach. *Arab J Sci Eng* 2018;43(3):1291–300. <https://doi.org/10.1007/s13369-017-2823-5>.
- [38] Chukwuezie OC, Nwaigwe KN, Asoegwu SN, Anyanwu EE. Diesel engine performance of jatropa biodiesel: a review. *Biofuels Taylor and Francis Ltd* 2014; 5(4):415–30. <https://doi.org/10.1080/17597269.2014.986416>.
- [39] Chauhan BS, Kumar N, Cho HM, Lim HC. A study on the performance and emission of a diesel engine fueled with Karanja biodiesel and its blends. *Energy* 2013;56:1–7. <https://doi.org/10.1016/j.energy.2013.03.083>.
- [40] Keera ST, El Sabagh SM, Taman AR. Castor oil biodiesel production and optimization. *Egypt J Pet* 2018;27(4):979–84. <https://doi.org/10.1016/j.ejpe.2018.02.007>.
- [41] Kishore Pandian A, Munuswamy DB, Radhakrishana S, Bathey Ramakrishnan RB, Nagappan B, Devarajan Y. Influence of an oxygenated additive on emission of an engine fueled with neat biodiesel. *Pet Sci* 2017;14(4):791–7. <https://doi.org/10.1007/s12182-017-0186-x>.
- [42] Gail S, Sarathy SM, Thomson MJ, Diévert P, Dagaut P. Experimental and chemical kinetic modeling study of small methyl esters oxidation: methyl (E)-2-butenate and methyl butanoate. *Combust Flame* 2008;155(4):635–50. <https://doi.org/10.1016/j.combustflame.2008.04.007>.
- [43] Teruel MA, Benitez-Villalba J, Caballero N, Blanco MB. Gas-phase oxidation of methyl crotonate and ethyl crotonate. Kinetic study of their reactions toward OH radicals and Cl atoms. *J Phys Chem A* 2012;116(24):6127–33. <https://doi.org/10.1021/jp2113889>.
- [44] Xi J, Zhong BJ. Soot in diesel combustion systems. *Chem Eng Technol* 2006;29(6):665–73. <https://doi.org/10.1002/ceat.200600016>.
- [45] Liu S, Wu X, Weng D, Ran R. Ceria-based catalysts for soot oxidation: a review. *J Rare Earths* 2015;33(6):567–90. [https://doi.org/10.1016/S1002-0721\(14\)60457-9](https://doi.org/10.1016/S1002-0721(14)60457-9).
- [46] Botero ML, Mosbach S, Kraft M. Sooting tendency of paraffin components of diesel and gasoline in diffusion flames. *Fuel* 2014;126:8–15. <https://doi.org/10.1016/J.FUEL.2014.02.005>.
- [47] Friedman HL. Kinetics of thermal degradation of char-forming plastics from thermogravimetry. Application to a phenolic plastic. *J Polym Sci Part C Polym Symp* 2007;6(1):183–95. <https://doi.org/10.1002/polc.5070060121>.
- [48] Vyazovkin S, Burnham AK, Criado JM, Pérez-Quageda LA, Popescu C, Sbirrazzuoli N. ICTAC Kinetics Committee recommendations for performing kinetic computations on thermal analysis data. *Thermochim Acta Elsevier* 2011;520(1–2):1–19. <https://doi.org/10.1016/j.tca.2011.03.034>.
- [49] Meng Z, Yang D, Yan Y. Study of carbon black oxidation behavior under different heating rates. *J Therm Anal Calorim* 2014;118(1):551–9. <https://doi.org/10.1007/s10973-014-4020-z>.
- [50] Man XJ, Cheung CS, Ning Z, Yung KF. Effect of waste cooking oil biodiesel on the properties of particulate from a DI diesel engine. *Aerosol Sci Technol* 2015;49(4):199–209. <https://doi.org/10.1080/02786826.2015.1016214>.

- [51] Sharma HN, Pahalagedara L, Joshi A, Suib SL, Mhadeshwar AB. Experimental study of carbon black and diesel engine soot oxidation kinetics using thermogravimetric analysis. *Energy Fuels* 2012;26(9):5613–25. <https://doi.org/10.1021/ef3009025>.
- [52] Fredrik Ahlström A, Ingemar Odenbrand CU. Combustion characteristics of soot deposits from diesel engines. *Carbon Pergamon* 1989;27(3):475–83. [https://doi.org/10.1016/0008-6223\(89\)90080-8](https://doi.org/10.1016/0008-6223(89)90080-8).
- [53] Raj A, Tayouo R, Cha D, Li L, Ismail MA, Chung SH. Thermal fragmentation and deactivation of combustion-generated soot particles. *Combust Flame* 2014;161(9):2446–57. <https://doi.org/10.1016/j.combustflame.2014.02.010>.
- [54] Raj A, da Silva GR, Chung SH. Reaction mechanism for the free-edge oxidation of soot by O₂. *Combust Flame* 2012;159(11):3423–36. <https://doi.org/10.1016/j.combustflame.2012.06.004>.
- [55] Chaparala SV, Raj A. Reaction mechanism for the oxidation of zigzag site on polycyclic aromatic hydrocarbons in soot by O₂. *Combust Flame* 2016;165:21–33. <https://doi.org/10.1016/j.combustflame.2015.09.012>.
- [56] Dobbins RA, Megaridis CM. Morphology of flame-generated soot as determined by thermophoretic sampling. *Langmuir* 1987;3(2):254–9. <https://doi.org/10.1021/la00074a019>.
- [57] Das DD, McEnally CS, Pfefferle LD. Sooting tendencies of unsaturated esters in nonpremixed flames. *Combust Flame* 2015;162(4):1489–97. <https://doi.org/10.1016/j.combustflame.2014.11.012>.
- [58] Appel J, Bockhorn H, Frenklach M. Kinetic modeling of soot formation with detailed chemistry and physics: laminar premixed flames of C₂ hydrocarbons. *Combust Flame* 2000;121(1–2):122–36. [https://doi.org/10.1016/S0010-2180\(99\)00135-2](https://doi.org/10.1016/S0010-2180(99)00135-2).
- [59] Joshi SP, Seal P, Pekkanen TT, Timonen RS, Eskola AJ. Direct kinetic measurements and master equation modelling of the unimolecular decomposition of resonantly-stabilized CH₂CHCHC(O)OCH₃ radical and an upper limit determination for CH₂CHCHC(O)OCH₃+ O₂ reaction. *Zeitschrift für Phys Chemie* 2020;234(7–9):1251–68. <https://doi.org/10.1515/zpch-2020-1612>.
- [60] Akbar Ali M, Violi A. Reaction pathways for the thermal decomposition of methyl butanoate. *J Org Chem* 2013;78(12):5898–908. <https://doi.org/10.1021/jo400569d>.
- [61] Yehliu K, Vander Wal RL, Boehman AL. Development of an HRTEM image analysis method to quantify carbon nanostructure. *Combust Flame* 2011;158(9):1837–51. <https://doi.org/10.1016/j.combustflame.2011.01.009>.
- [62] Pfau SA, La Rocca A, Fay MW. Quantifying soot nanostructures: importance of image processing parameters for lattice fringe analysis. *Combust Flame* 2020;211:430–44. <https://doi.org/10.1016/J.COMBUSTFLAME.2019.10.020>.
- [63] Lapuerta M, Rodríguez-Fernández J, Sánchez-Valdepeñas J. Soot Reactivity analysis and implications on diesel filter regeneration. *Prog Energy Combust Sci Elsevier Ltd* 2020;78:100833. <https://doi.org/10.1016/j.pecs.2020.100833>.
- [64] Grisdale RO. The formation of black carbon. *J Appl Phys* 1953;24(9):1082–91. <https://doi.org/10.1063/1.1721452>.
- [65] Catelani T, Pratesi G, Zoppi M. Raman characterization of ambient airborne soot and associated mineral phases. *Aerosol Sci Technol* 2014;48(1):13–21. <https://doi.org/10.1080/02786826.2013.847270>.
- [66] Lapuerta M, Oliva F, Agudelo JR, Boehman AL. Effect of fuel on the soot nanostructure and consequences on loading and regeneration of diesel particulate filters. *Combust Flame* 2012;159(2):844–53. <https://doi.org/10.1016/j.combustflame.2011.09.003>.
- [67] Ferrari A, Robertson J. Interpretation of Raman spectra of disordered and amorphous carbon. *Phys Rev B - Condens Matter Mater Phys* 2000;61(20):14095–107. <https://doi.org/10.1103/PhysRevB.61.14095>.
- [68] Escribano R, Sloan JJ, Siddique N, Sze N, Dudev T. Raman spectroscopy of carbon-containing particles. *Vib Spectrosc* 2001;26(2):179–86. [https://doi.org/10.1016/S0924-2031\(01\)00106-0](https://doi.org/10.1016/S0924-2031(01)00106-0).
- [69] Raj A. Structural effects on the growth of large polycyclic aromatic hydrocarbons by C₂H₂. *Combust Flame* 2019;204:331–40. <https://doi.org/10.1016/j.combustflame.2019.03.027>.
- [70] Raj A, Yang SY, Cha D, Tayouo R, Chung SH. Structural effects on the oxidation of soot particles by O₂: experimental and theoretical study. *Combust Flame* 2013;160(9):1812–26. <https://doi.org/10.1016/j.combustflame.2013.03.010>.
- [71] Yehliu K, Vander Wal RL, Armas O, Boehman AL. Impact of fuel formulation on the nanostructure and reactivity of diesel soot. *Combust Flame* 2012;159(12):3597–606. <https://doi.org/10.1016/j.combustflame.2012.07.004>.
- [72] Lapuerta M, Rodríguez-Fernández J, Sánchez-Valdepeñas J, Salgado MS. Multi-technique analysis of soot reactivity from conventional and paraffinic diesel fuels. *Flow, Turbul Combust* 2016;96(2):327–41. <https://doi.org/10.1007/s10494-015-9644-y>.
- [73] Dooley S, Curran HJ, Simmie JM. Autoignition measurements and a validated kinetic model for the biodiesel surrogate, methyl butanoate. *Combust Flame* 2008;153(1–2):2–32. <https://doi.org/10.1016/j.combustflame.2008.01.005>.
- [74] Zhou X, Zhai Y, Ye L, Zhang L. Theoretical studies on the reaction kinetics of methyl crotonate with hydroxyl radical. *Sustain Energy Fuels* 2018;2(2):392–402. <https://doi.org/10.1039/c7se00426e>.
- [75] Bennadji H, Coniglio L, Billaud F, Bounaceur R, Warth V, Glaude P-A, et al. Oxidation of small unsaturated methyl and ethyl esters. *Int J Chem Kinet* 2011;43(4):204–18. <https://doi.org/10.1002/kin.20536>.
- [76] Gail S, Thomson MJ, Sarathy SM, Syed SA, Dagaut P, Diévert P, et al. A wide-ranging kinetic modeling study of methyl butanoate combustion. *Proc Combust Inst* 2007;31(1):305–11. <https://doi.org/10.1016/j.proci.2006.08.051>.
- [77] Kalvakala KC, Katta VR, Aggarwal SK. Effects of oxygen-enrichment and fuel unsaturation on soot and NO_x emissions in ethylene, propane, and propene flames. *Combust Flame* 2018;187:217–29. <https://doi.org/10.1016/j.combustflame.2017.09.015>.